

MR Imaging of Congenital Heart Diseases in Adolescents and Adults

Yeon Hyeon Choe, MD¹
I-Seok Kang, MD²
Seung Woo Park, MD²
Heung Jae Lee, MD²

Echocardiography and catheterization angiography suffer certain limitations in the evaluation of congenital heart diseases in adults, though these are overcome by MRI, in which a wide field-of view, unlimited multiplanar imaging capability and three-dimensional contrast-enhanced MR angiography techniques are used. In adults, recently introduced fast imaging techniques provide cardiac MR images of sufficient quality and with less artifacts. Ventricular volume, ejection fraction, and vascular flow measurements, including pressure gradients and pulmonary-to-systemic flow ratio, can be calculated or obtained using fast cine MRI, phase-contrast MR flow-velocity mapping, and semiautomatic analysis software. MRI is superior to echocardiography in diagnosing partial anomalous pulmonary venous connection, unroofed coronary sinus, anomalies of the pulmonary arteries, aorta and systemic veins, complex heart diseases, and postsurgical sequelae. Biventricular function is reliably evaluated with cine MRI after repair of tetralogy of Fallot, and Senning's and Mustard's operations. MRI has an important and growing role in the morphologic and functional assessment of congenital heart diseases in adolescents and adults.

Index terms :

Heart, MR
Heart, diseases
Heart, congenital anomalies

Korean J Radiol 2001 ;2: 121-131

Received March 10, 2001; accepted after revision July 20, 2001.

Department of ¹Radiology and ²Grown-up Congenital Heart Disease Clinic, Cardiac and Vascular Center, Samsung Medical Center, Sungkyunkwan University School of Medicine, Seoul, Korea

This paper was supported in part by Samsung Medical Center and Sungkyunkwan University.

Address reprint requests to:

Yeon Hyeon Choe, MD, Department of Radiology, Samsung Medical Center, Sungkyunkwan University School of Medicine, 50 Ilwon-dong, Kangnam-gu, Seoul 135-710, Korea.
Telephone: (822) 3410-2509
Fax: (822) 3410-2559
e-mail: yhchoe@smc.samsung.co.kr

MRI has proven valuable for the diagnosis of various congenital heart diseases (CHD) (1–22). To date, its use in the evaluation of such diseases has, however, been limited, though recent technical developments in MRI have provided new opportunities for its wider application in cardiac imaging. Dedicated cardiac MRI equipment as well as deliberate cardiac coils, fast imaging techniques, cardiac function analysis tools and contrast-enhanced MR angiography are all now available (23, 24). At this time, the role of MRI in CHD should be reestablished on the basis of the experiences of the past and the possibilities of the future made real by these new procedures.

Due to improvements in therapeutic techniques, the number of adult patients with CHD is increasing. Because the acoustic window for transthoracic echocardiography is limited in adults, the reliability of echocardiography decreases with age. Transesophageal echocardiography overcomes most limitations of the transthoracic mode, but is a semi-invasive technique and thorough imaging of the aortic arch, pulmonary arteries, and some systemic and pulmonary veins is hindered by airways and lungs. MRI provides excellent definition of extracardiac anomalies as well as clear depiction of intracardiac anomalies (25–28), and is also useful in the evaluation of ventricular function and the assessment of flow velocity and volume. A combination of echocardiography and MRI may obviate the need for catheter cardiac angiography in young adults with congenital heart diseases. This review article describes current techniques in MRI of CHD and MRI findings pertaining to specific anomalies in which the modality is useful in diagnosis.

Techniques

In most patients, a cardiac surface coil usually provides good signals, though a body coil or torso phased-array receiver coil may be used instead. ECG-gated multislice spin-echo images, double inversion-recovery images (TE = 40 ms) and breath-hold fast cine images are obtained. Respiratory gating is applied during spin-echo imaging, and for T1-weighted spin-echo or double inversion-recovery images in adults, a slice thickness of 5–10 mm is used.

The details of conventional and newer fast cardiac MR imaging techniques have been described elsewhere (29, 30). Gradient-echo techniques have been used for cine MR imaging (TR/TE = 20–30 ms/5–12 ms, flip angle = 30°). Cine MR imaging using gradient echo techniques takes 3–6 min depending on heart rates, and fast cine techniques (TR/TE = 7.7–8.0 ms/4.3–4.5 ms), in which images with more than 30 phases per cardiac cycle can be acquired during a single breath-hold period, have recently been introduced. The endocardial edge is more easily detected using specially designed gradient-echo sequences such as true FISP (fast imaging with steady precession), balanced fast field-echo, and FIESTA (fast imaging employing steady-state acquisition) (TR/TE = 4.1–5.1 ms/1.8–2.1 ms). The true FISP or FIESTA technique preserves the coherence of transverse magnetization by refocusing gradients in all three axes (30). Because both transverse and longitudinal magnetization reach a steady-state equilibrium, image signal-to-noise ratio with these techniques is greater than with the spoiled gradient-echo sequence. The true FISP or FIESTA technique gives excellent blood-tissue contrast, minimizes artifacts due to blood flow, and renders semi-automatic detection of endocardial edge more reliable and

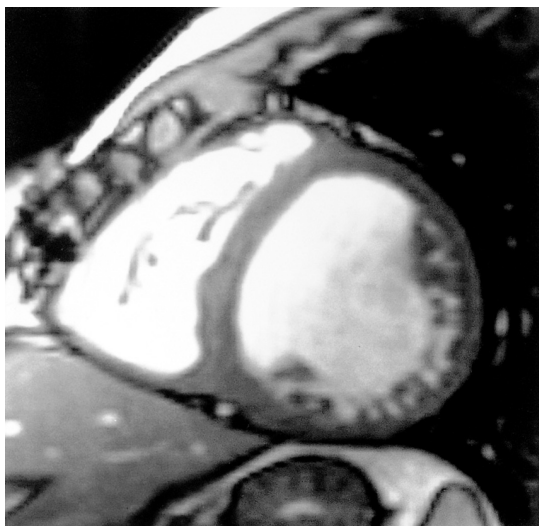


Fig. 1. Diastolic phase short-axial image obtained using the FIESTA technique shows excellent blood-tissue contrast.

faster (Fig. 1). Hartnell et al. (27) described a modified cine technique. A user-defined 90° RF presaturation pulse followed by a spoiler gradient is positioned through the chamber thought to be a source of intracardiac shunt. Cine images are acquired after application of the saturation pulse in an orientation which can profile any shunt, which is revealed as flow of saturated blood (dark, low signal) across the structure under investigation.

Recently developed coronary MR angiography techniques can be applied to the imaging of coronary artery anomaly. Two-dimensional gradient-echo sequences with segmented k-space acquisition or three-dimensional contrast-enhanced MR angiography techniques are used with breath-holding or respiratory gating. Recent techniques also include spiral three-dimensional rapid gradient-echo using navigator techniques and diastolic gating.

Contrast-enhanced three-dimensional MR angiography is performed in the coronal or oblique sagittal plane using fast spoiled gradient-recalled echo techniques (TR/TE = 4.4–4.6 ms/0.9–1.0 ms, flip angle = 40°, field of view = 40 cm, matrix = 256 × 128–192, number of excitations = 1, slice thickness = 3–7.2 mm, zero interpolations = 4). Contrast material is provided by an automatic injector or by hand injection, and scanning is timed by automated contrast bolus detection or the time-resolved MR angiography technique (31, 32). Source and three-dimensional im-

Table 1. MR Imaging Planes Useful in the Evaluation of Individual Cardiovascular Anomalies

Anomalies	Imaging Planes	Reference Structures
PDA	Oblique sagittal	Main PA, descending aorta
CoA	Oblique sagittal	Aortic arch
PA abnormality	Oblique coronal	Both main PAs
PV abnormality	Coronal, axial	PVs
Palliative shunt	Coronal, axial	Shunt
Airways	Axial, sagittal	Trachea, main bronchi
Ventricular function	Short-axial	Ventricle
Subaortic stenosis	Short- and long-axial	Aortic valve
Unroofed CS	Oblique sagittal	CS
Complex heart disease	Axial, coronal, sagittal	Atria, ventricles, great vessels
ASD	Axial, oblique sagittal	Interatrial septum
VSD	Axial, coronal, sagittal, en-face view	Interventricular septum

Note.—ASD, atrial septal defect; CoA, coarctation of aorta; CS, coronary sinus; PA, pulmonary artery; PDA, patent ductus arteriosus, PV, pulmonary vein; VSD, ventricular septal defect

ages are helpful in understanding anomalies of the aorta and pulmonary vessels.

Information on blood flow velocity, pressure gradients, and flow volume through vessels, conduits, valves, and septal defects is provided by velocity-encoded cine MRI using a phase-contrast technique. Qp/Qs (ratio of pulmonary-to-systemic flow) can also be calculated using this technique (Fig. 2).

MR imaging planes should be selected appropriately according to individual anomalies (18): all three orthogonal planes (axial, coronal, and sagittal) are not always necessary; axial images are usually obtained first. MR imaging planes useful in the evaluation of individual anomalies are summarized in Table 1.

Partial Anomalous Pulmonary Venous Connections and Atrial Septal Defects

Overlying lungs may obscure pulmonary venous connections at echocardiography. Most patients with partial anomalous pulmonary venous connections (PAPVC) are asymptomatic and about half have atrial septal defects (33). Superior sinus venosus defect of the interatrial sep-

tum associated with PAPVC may simulate normal connection of the right upper pulmonary vein at catheterized right upper pulmonary venography. Oxymetry does not always demonstrate a step-up in oxygen saturation.

MRI can depict PAPVC in most patients (8, 14, 15, 23, 27, 28, 34). Ferrari et al. (23) reported predictive diagnostic accuracy of 100%, 80%, and 78% for ultrafast three-dimensional contrast-enhanced MR angiography with fast cine MRI, transesophageal echocardiography, and catheterization, respectively, in ten adults with PAPVC. Transesophageal echocardiography missed right-side PAPVC with high insertion of anomalous pulmonary veins to the superior vena cava (>2.0 cm above the right atrium) or left-side PAPVC to the left innominate vein. MRI appears to be the best noninvasive test for this anomaly (20). The connection site of individual pulmonary veins can be identified separately on MR images. Upper pulmonary veins are better visualized in the coronal or oblique coronal plane, and lower pulmonary veins in the axial or oblique sagittal plane (18). A defect in the wall of the superior vena cava ('broken ring' sign) (14) revealed by axial spin-echo or cine MR imaging may indicate PAPVC to the supe-

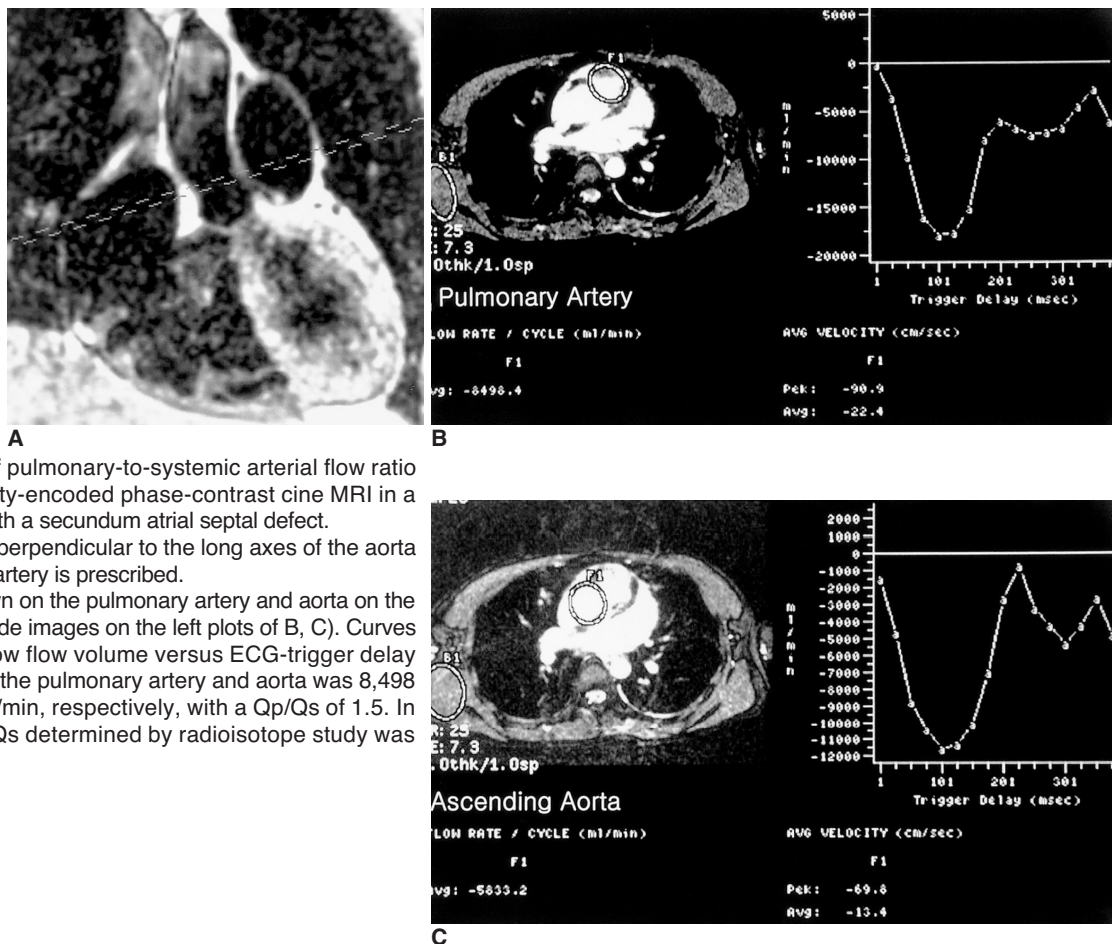


Fig. 2. Calculation of pulmonary-to-systemic arterial flow ratio (Qp/Qs) using velocity-encoded phase-contrast cine MRI in a 24-year-old female with a secundum atrial septal defect. **A.** An imaging plane perpendicular to the long axes of the aorta and main pulmonary artery is prescribed. **B, C.** ROIs were drawn on the pulmonary artery and aorta on the cine images (magnitude images on the left plots of B, C). Curves on the right plots show flow volume versus ECG-trigger delay time. Flow volume of the pulmonary artery and aorta was 8,498 ml/min and 5,833 ml/min, respectively, with a Qp/Qs of 1.5. In this patient, the Qp/Qs determined by radioisotope study was 1.7.

rior vena cava. Breath-hold cine MRI can easily demonstrate PAPVC if cine images of contiguous sections are acquired and viewed in paging in the axial and oblique coronal plane. Contrast-enhanced MR angiography is also very useful in the depiction of PAPVC (Fig. 3). Source and three-dimensional images can clearly visualize the connection sites of pulmonary veins and associated atrial septal defects.

In MR imaging of atrial septal defect, an oblique sagittal view tangential to the interatrial septum demonstrates this septum better than an axial view (35). However, spin-echo images can be unreliable in demonstrating interatrial septal defect: their sensitivity and specificity are 50% and 58%, respectively (27). Signal loss in the thin secundum septum simulates an atrial septal defect. Cine MRI can show intact septum in the fossa ovalis area, and according to Hartnell

et al. (27), cine MRI with selective presaturation can detect small atrial septal defects or patent oval foramen, ventricular septal defects, and patent arterial ducts. Hoppe et al. (28) found that both MRI and transesophageal echocardiography helped detect atrial septal defects in 36 of 37 patients, while transthoracic echocardiography demonstrated these defects in 24 of 37. High sinus venosus atrial septal defects cannot be fully visualized by transesophageal echocardiography (23), but this lesion can be depicted by MRI (Fig. 4).

Pulmonary Arterial Abnormalities

Echocardiography has a limited role in the evaluation of pulmonary arteries in adults. Selective catheterization and angiography of the pulmonary artery may not be possible when pulmonary stenosis is severe. MR imaging can be

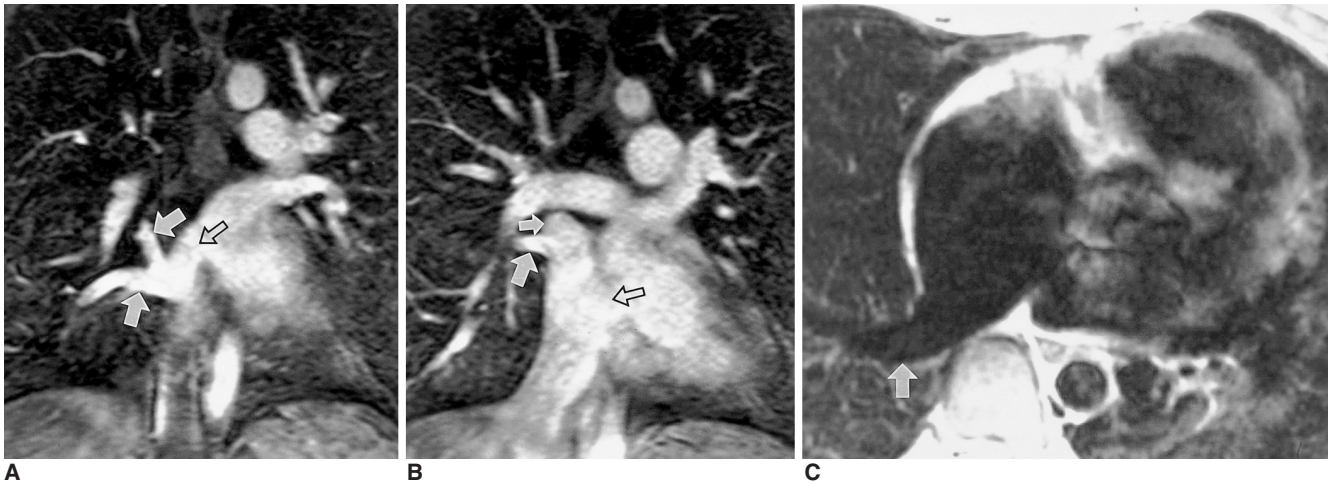


Fig. 3. 41-year-old female with partial anomalous pulmonary venous connection of right pulmonary veins to the right atrium and two atrial septal defects.
A, B. Coronal source images obtained by contrast-enhanced MR angiography clearly show right upper and middle pulmonary veins (solid arrows) connected with the right atrium. Two atrial septal defects (open arrows) are also visible.
C. Axial double inversion-recovery images show the right lower pulmonary vein (arrow) connected with the right atrium.

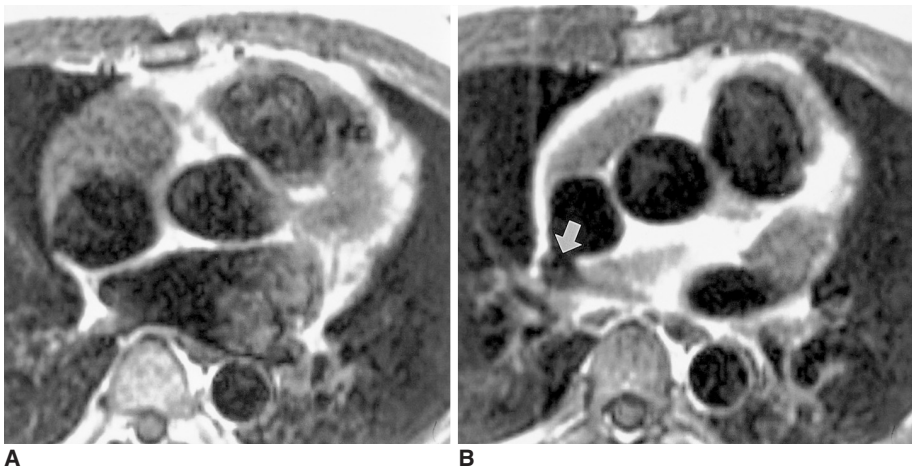


Fig. 4. Small, tricky, atrial septal defect in a 44-year-old male. Transthoracic and transesophageal echocardiography failed to depict the atrial septal defect in spite of clinical suspicion of a left-to-right shunt.
A. Axial spin-echo MR image shows intact interatrial septum at the level of the aortic valve.
B. Spin-echo image cephalad to A shows a small defect (arrow) in the periphery of the interatrial septum near the junction with the superior vena cava.

useful in the noninvasive evaluation of the pulmonary arterial tree before and after surgical treatment of cyanotic heart diseases in young adults (28, 35). In these patients, existing pulmonary arterial morphology crucially affects the planning of surgical correction or palliation. Oblique coronal planes parallel to the pulmonary arterial long axes are better than axial planes for determining the diameters of pulmonary arteries. In the evaluation of pulmonary arterial anomalies, contrast-enhanced MR angiography provides the most information (Fig. 5).

In patients with pulmonary atresia, multiple collateral arteries can be identified using three-dimensional contrast-enhanced MR angiography (Fig. 6). The source images ob-

tained in coronal planes also visualize collateral arteries arising from the descending thoracic aorta. Central pulmonary arteries are depicted at spin-echo MRI, breath-hold cine MRI, and contrast-enhanced MR angiography.

Various palliative shunts, including the cavopulmonary, modified Blalock-Taussig, and central types can be reliably evaluated with MRI. In patients with proximal interruption of unilateral pulmonary artery or in those with pulmonary atresia and occluded palliative shunts, catheter angiography may fail to visualize the distal pulmonary artery or central pulmonary arteries. In these situations, MRI may be useful in the depiction of these arteries (13, 22).

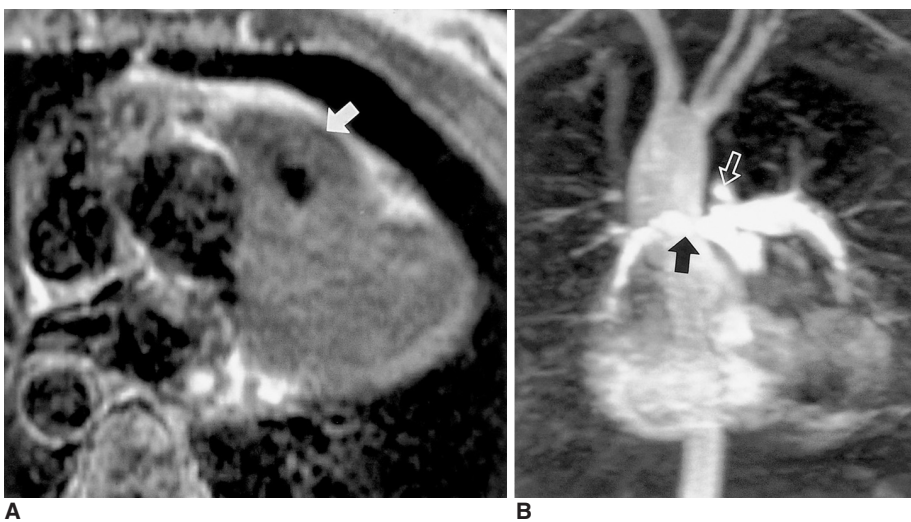


Fig. 5. Tetralogy of Fallot in a 37-year-old female. MRI rather than catheter angiography was performed prior to surgery.

A. Axial spin-echo MR image shows severe infundibular stenosis (arrow).
B. Three-dimensional contrast-enhanced MR angiography shows small right pulmonary artery (solid arrow) and a ductus diverticulum (open arrow). Note, too, the right-sided aortic arch with mirror image branching.

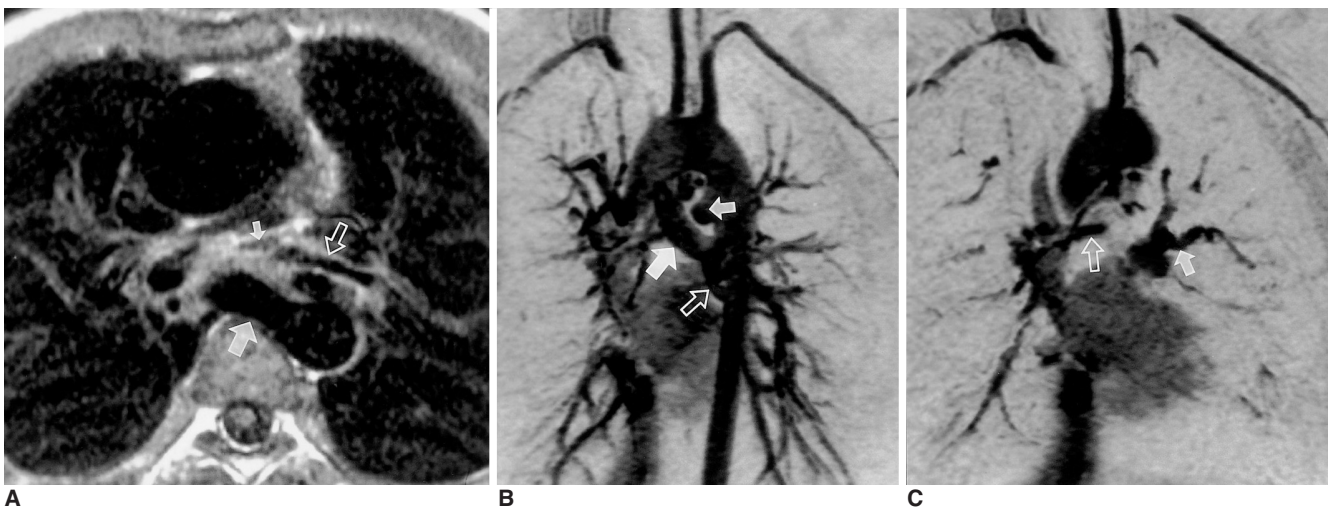


Fig. 6. Pulmonary atresia with ventricular septal defect in a 14-year-old female. MRI was performed to evaluate the size and number of aortopulmonary collateral arteries and to verify the presence of central pulmonary arteries (**A**, spin-echo image; **B** and **C**, three-dimensional images obtained by contrast-enhanced MR angiography with partial volume reconstruction). A major collateral aortopulmonary artery (large solid arrow in **A**, **B**) arises from the descending thoracic aorta. Note, too, the presence of another collateral artery (small solid arrow in **B**) just distal to the aortic arch and small collateral arteries (open arrows in **A**, **B** and solid arrow in **C**). Small central pulmonary arteries (small arrow in **A**, open arrow in **C**) with stenosis in the confluent segment are demonstrated by spin-echo imaging and three-dimensional MR angiography.

Aortic Abnormalities

Coarctation of the aorta can be accurately diagnosed at MRI (6, 28), with spin-echo imaging in the axial and oblique sagittal planes usually providing sufficient information. Kinking of the aorta, as seen in patients with aortic pseudocoarctation, may cause apparent stenosis (36). Fast cine MR imaging can show signal loss due to turbulent flow at the coarctation segment or in, above and below the aortic valve area. Three-dimensional contrast-enhanced MR angiography is performed in the oblique sagittal plane and helps provide an understanding of these anomalies (Fig. 7). The identification of collateral vessels at MR angiography may be useful in planning surgical treatment of this anomaly. Velocity-encoded cine MRI also gives information on the severity of the stenosis and pressure gradient across the coarctation. The amount of collateral flow in the aorta distal to the stenotic segment can be assessed by measuring flow volume in the aorta just distal to the stenosis and at the level of the diaphragm.

A bicuspid aortic valve and subaortic stenosis may be associated with coarctation or interruption of the aortic arch. The causes of subaortic stenosis include fibromuscular ridge and hypertrophy of the anterolateral muscle or interventricular septum, and the condition is best visualized on short- or long-axial spin-echo (double inversion-recovery) or cine images (18) (Fig. 8). MRI is able to provide true short-axis images in the subaortic region.

Supravalvular aortic stenosis, interruption of the aortic arch, cervical or double aortic arch, aberrant subclavian artery, truncus arteriosus, hemitruncus arteriosus, and aor-

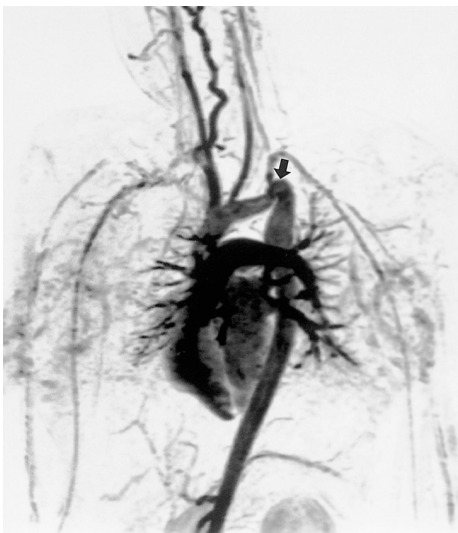


Fig. 7. Tubular hypoplasia of the aortic arch and coarctation in a 17-year-old female. Maximal intensity projection image obtained by contrast-enhanced MR angiography clearly shows arch hypoplasia and coarctation (arrow). This patient also suffered intracerebral hemorrhage, probably associated with coarctation.

topulmonary window can also be correctly diagnosed with MRI (16, 28). Coronal spin-echo or cine MR images show supravalvular aortic stenosis and left ventricle hypertrophy. In patients with vascular rings or low-lying aortic arches, tracheal compression or stenosis is frequently associated. Axial and sagittal MR images show tracheobronchial abnormalities as well as vascular anomalies.



Fig. 8. Subaortic stenosis associated with coarctation of the aorta in a 14-year-old male. Short-axis spin-echo MR image demonstrates subaortic stenosis (SA) due to hypertrophied anterolateral muscle (M).

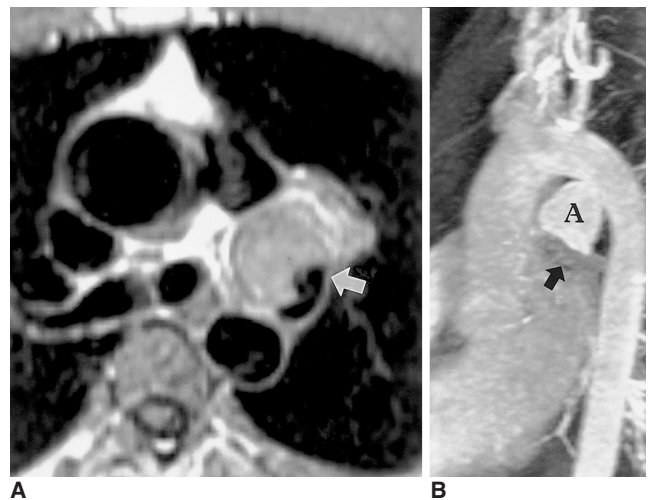


Fig. 9. Aneurysm of the ductus arteriosus in a 31-year-old male. **A.** Axial spin-echo MR image shows a large aneurysm (arrow) with slow flow within. Spin-echo images do not clearly indicate the origin of this aneurysm. **B.** Three-dimensional contrast-enhanced MR angiography depicts a bell-shaped aneurysm (A) connected with the aorta. Poor opacification of the hypoplastic left pulmonary artery (arrow) suggests closure of the pulmonary arterial end of the ductus arteriosus.

Patent Ductus Arteriosus

Due to limited acoustic access, patent ductus arteriosus in adults can be missed at transthoracic or transesophageal echocardiography with color flow mapping (28), and the condition is best depicted by oblique sagittal cine MRI. Signal void in the main pulmonary artery on cine MR images may suggest the presence of a patent arterial duct. After spontaneous closure of the aortic or pulmonary arterial end of this, a diverticulum may develop in the main pulmonary artery or aorta. True aneurysm of an arterial duct is rare, though three-dimensional contrast-enhanced MR angiography can reveal the ductal origin of an aneurysm (Fig. 9).

Patent ductus arteriosus may cause marked enlargement and even rupture of the pulmonary artery. The jet flow

through the ductus arteriosus evokes intimal injury of the main pulmonary artery and subsequent endocarditis and pseudoaneurysm (37). Axial and coronal spin-echo MR images and contrast-enhanced MR angiography can reveal the patent ductus arteriosus and a pseudoaneurysm of the pulmonary artery.

Ventricular Septal Defect

Most ventricular septal defects can be correctly diagnosed with MRI (28). According to Hoppe et al. (28), MRI detected ventricular septal defects in 14 of 15 patients, proving superior to transesophageal echocardiography (detection in 12 of 15 patients) and comparable to transthoracic echocardiography (detection in 14 of 15 patients).

Small muscular septal defects can be missed on spin-echo

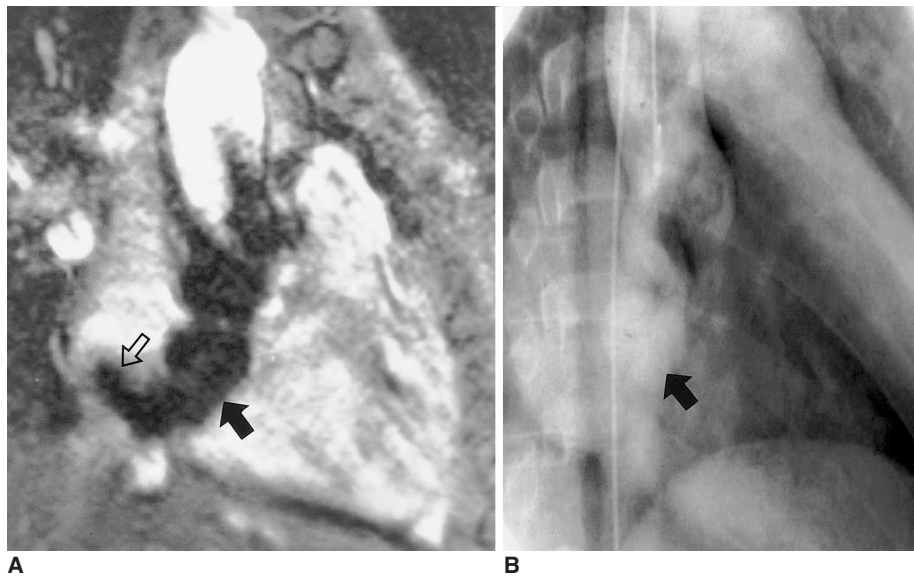


Fig. 10. Rupture of an aneurysm of the sinus of Valsalva in a 42-year-old male. **A.** Cine MR image in the oblique coronal plane. Turbulent flow (open arrow) is demonstrated as signal voids in the right atrium emanating from the tip of the 'windsock' (solid arrow). **B.** Conventional cine angiography performed after MRI also shows the ruptured aneurysm of the coronary sinus. Due to low image contrast between the cardiac chambers and aneurysm, the 'windsock' is barely perceptible, however. Surgical findings confirmed the presence of a 4-cm long aneurysm of the sinus of Valsalva and a 0.5-cm-sized tear at the tip of the aneurysm.

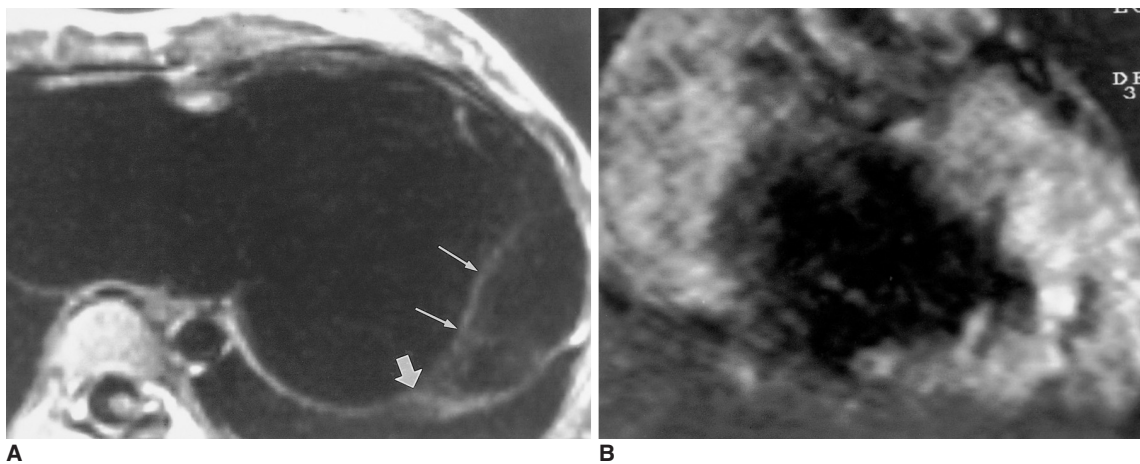


Fig. 11. Ebstein's anomaly of the tricuspid valve in a 17-year-old female. **A.** Oblique axial spin-echo image shows displaced attachment (thick arrow) of the posterior leaflet (thin arrows). **B.** Conventional cine MR image in the oblique coronal plane shows a large signal void area due to severe tricuspid regurgitation.

images. Cine MRI is useful in the detection of signal void due to high-velocity jet from muscular or subarterial ventricular septal defects. MRI may depict a septal aneurysm associated with a perimembranous ventricular septal defect.

Rupture of the Sinus of Valsalva Aneurysm

Cine MRI is very useful in depicting this anomaly. Turbulent flow through the 'windsock' of the aneurysmal sinus of Valsalva and its defect are easily visible on cine MRI (Fig. 10). Multiple oblique coronal and axial cine images visualize the turbulent flow and defects in the sinus and interventricular septum.

Ebstein's Anomaly

Ebstein's anomaly, which in adults is less severe than in infants and children, may be missed if poor acoustic access limits clear visualization of the tricuspid valve at transthoracic echocardiography. Cine MRI demonstrates tricuspid regurgitation and displaced attachment of septal and posterior leaflets (Fig. 11). Spin-echo (or double inversion-recovery) and cine MRI are performed in the oblique axial, oblique coronal, and sagittal planes (21). The functioning of the right ventricle can be assessed by means of short-axis cine imaging. Axial images are most informative and show septal and anterior leaflets of the tricuspid valve, atrialized right ventricle, functioning right ventricle, and infundibulum (21). Coronal images show the posterior leaflet of the tricuspid valve. MRI can visualize thinning of the

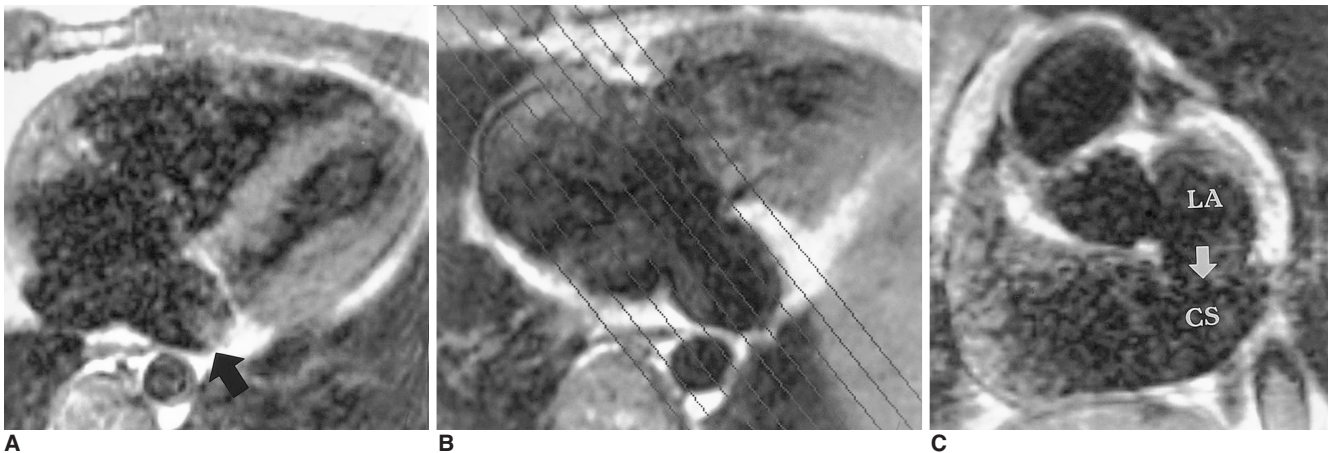


Fig. 12. Unroofed coronary sinus in a 24-year-old male.

A. Axial spin-echo MR image shows an enlarged coronary sinus (arrow).

B, C. Oblique sagittal planes were selected for imaging of the coronary sinus and left atrium.

C. Coronary sinus view, as prescribed in B, shows a large defect (arrow) in the wall between the coronary sinus (CS) and left atrium (LA).

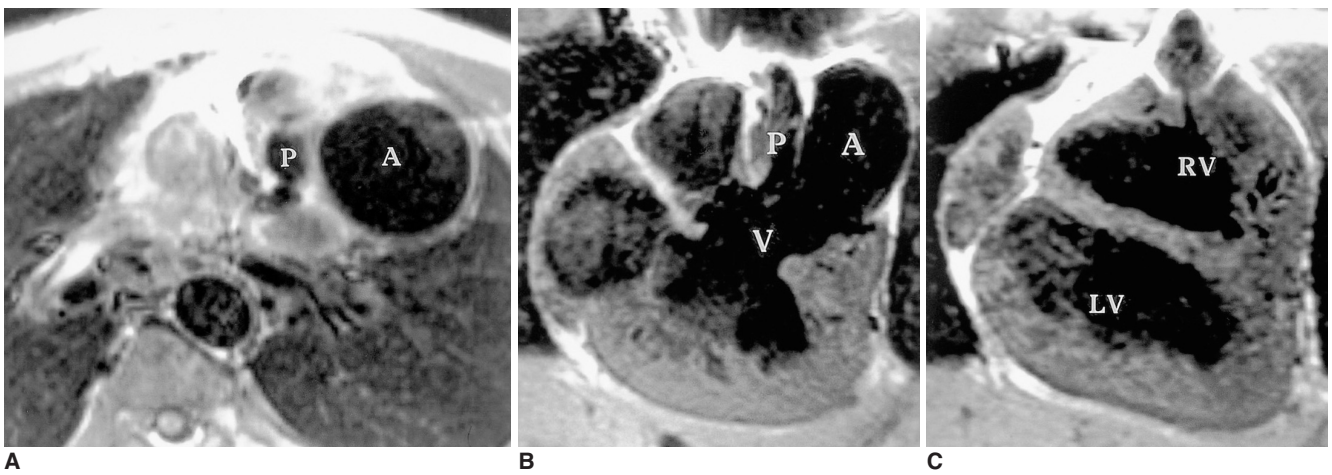


Fig. 13. Corrected transposition in a 14-year-old male.

A. Axial spin-echo image shows the left-sided aorta (A) alongside the hypoplastic pulmonary artery (P).

B, C. Coronal spin-echo images show a large ventricular septal defect (V) and aorta (A) arising from the left-sided and superiorly located hypoplastic right ventricle (RV). LV, left ventricle

atrialized right ventricle, stenosis of the tricuspid valve, and associated atrial septal defects.

Persistent Left Superior Vena Cava and Unroofed Coronary Sinus

Anomalies of the left superior vena cava, a vein connected with the coronary sinus or directly with the left atrial roof, are relatively common. Recognition of this anomaly is important before cavopulmonary shunt or Fontan's operation. Axial and coronal spin-echo images depict the left superior vena cava and dilated coronary sinus.

Unroofed coronary sinus, an anomaly usually associated with a left superior vena cava connecting to the left atrium, is rare, and presents with defects in the wall between this and the coronary sinus. The defects may vary in size and be multiple.

Echocardiography may miss the fenestrations, though the dilated coronary sinus is easily visible. For demonstration of this anomaly, spin-echo and cine MR images in oblique sagittal or cardiac short-axial planes along the long axis of the coronary sinus are useful (Fig. 12).

Anomalies of Coronary Arteries

Recently introduced fast imaging techniques permit coronary artery imaging (24). Although only the proximal segments of coronary arteries can be reliably visualized with this breath-hold spiral k-space acquisition technique, diagnosis of the variations or anomalies of coronary artery origination is feasible (24, 27). According to Taylor et al. (24), respiration-gated MR coronary angiography had an accuracy of 92%, a sensitivity of 88%, and a specificity of 100% in the detection of anomalous coronary arteries in 16 patients.

Coronary arteriovenous fistula can be seen on axial and coronal images as the presence of dilated and tortuous

anomalous vessels around the pulmonary artery or cardiac chambers.

Complex Heart Diseases

Corrected transposition, twisted atrioventricular connection, tricuspid atresia or univentricular atrioventricular connection rarely present in adulthood. MRI can be useful in the evaluation of atriobronchial situs by direct imaging of these structures. Abnormal arterial, venous and atrioventricular connections can be sought and assessed by axial, sagittal, and coronal MR imaging (Fig. 13). MRI has an important role in demonstrating ventricular anatomy in complex heart diseases (9, 10, 20).

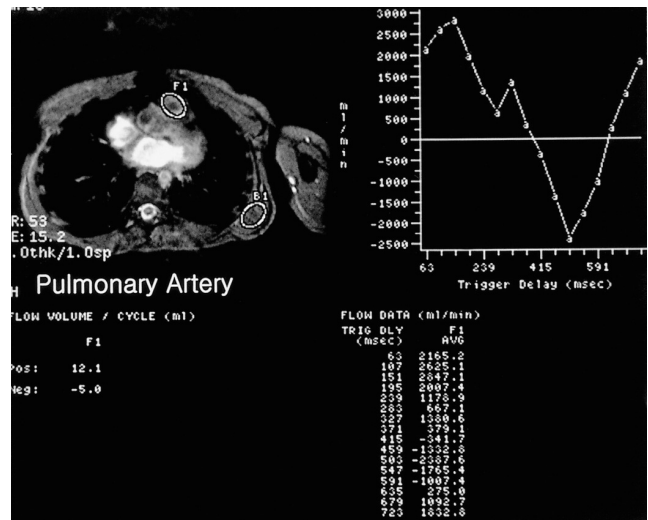


Fig. 15. Estimation of the severity of pulmonary regurgitation after repair of tetralogy of Fallot using velocity-encoded cine MRI. The curve on the right plots pulmonary arterial flow against ECG-trigger delay time. The area between the baseline and the curve below the baseline represents regurgitant volume.

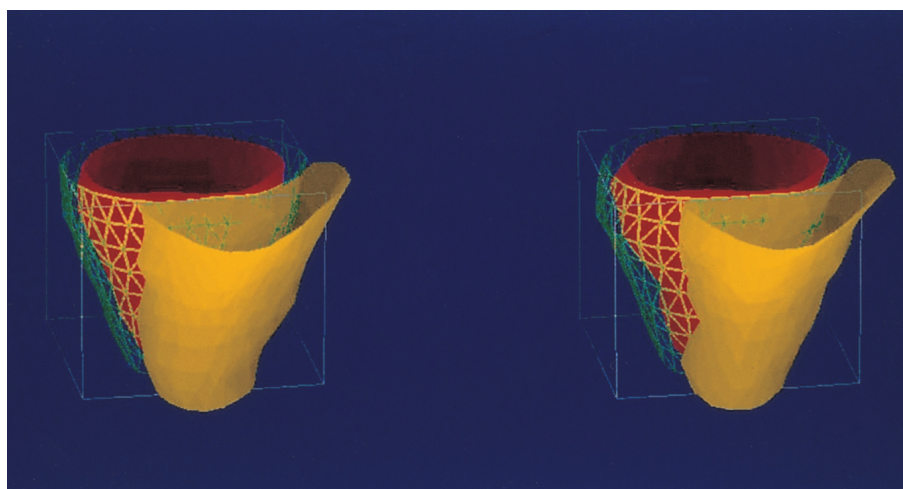


Fig. 14. Biventricular function evaluation using fast cine MR imaging and semi-automated ventricular function analysis software. This 22-year-old male has undergone surgical repair for tetralogy of Fallot and now presents with decreased biventricular function and pulmonary regurgitation. The figure shows three-dimensional images of the right (yellow) and left (red) ventricles in diastolic (left image) and systolic (right image) phases. The three-dimensional volume ejection fraction calculated by this technique was 20.1% and 20.0% for right and left ventricles, respectively.

Postsurgical Morphology

Transthoracic echocardiography has a limited role in post-surgical patients. Scar tissue hinders proper evaluation of the postoperative status of CHDs. Where extracardiac ventriculopulmonary shunts or conduits are located retrosternally, transthoracic echocardiography is difficult.

MRI is particularly valuable in the evaluation of surgical complications in various CHDs (19, 20, 25–28), and can be helpful in assessing the size of the cardiac chambers and great vessels, the status of anastomosis, shunt patency, the presence of stenosis or occlusion of the pulmonary artery or conduit, pseudoaneurysms of the aorta or pulmonary artery after repair of coarctation or tetralogy of Fallot, thrombi or vegetations, and compression of the pulmonary vein or bronchus by an enlarged atrium or great vessels.

Functional Evaluation

Cine MR imaging is useful in the evaluation of ventricular function and valvular competency in patients with CHD before and after surgical correction. In many CHDs, right ventricular function is important in determining the outcome. Three-dimensional volume, mass, and ejection fraction can be accurately calculated using contiguous short-axis cine images covering all left or right ventricular dimensions (19, 20, 38). This is particularly helpful after Mustard's or Senning's operation.

Right and left ventricular dysfunction is associated with pulmonary regurgitation after repair of tetralogy of Fallot. In such patients, biventricular function and mass can be assessed with cine MRI, and pulmonary regurgitation with phase-contrast MR flow-velocity mapping (19) (Figs 14, 15).

Comparison of the Value of MRI and Echocardiography in Adults

A small number of published articles have dealt with this topic (23, 26–28). According to Hoppe et al. (28), transthoracic echocardiography demonstrated 75.2% of 344 abnormalities, transesophageal echocardiography, 83%, and MR imaging, 92% in 61 patients. MRI was the only technique to fully depict 31 extracardiac anomalies. Transesophageal echocardiography best depicted the atrioventricular junction and atrial structures, while in cases with complex cardiac defects, the combination of all three imaging techniques was most effective. Abnormalities were missed due to poor image quality in three, eleven, and two patients who underwent MR imaging, transthoracic and transesophageal echocardiography, respectively. Hartnell et al. (27) compared the usefulness of time-of-flight MR angiography and breath-hold fast cine MRI with that of spin-echo MRI in 49 adults with CHDs. MR angiography demonstrated or excluded all confirmed congenital valve

(12/12), aortic (9/9), and venous (7/7) anomalies and detected most confirmed shunts (31/33), while spin-echo MRI, with a specificity of 58%, was unreliable in demonstrating shunts.

CONCLUSIONS

MRI is the modality of choice in the diagnosis of anomalies of pulmonary arterial trees, pulmonary veins, and the aortic arch, as well as in the evaluation of complex heart diseases and post-surgical morphology in adult patients. MRI is complementary to transthoracic and transesophageal echocardiography in the evaluation of intracardiac anomalies. The volume, mass, and ejection fraction of the right and left ventricles, along with wall motion and thickness analysis, can be determined using fast cine MRI. Pressure gradient and volume flow through stenotic vessels and shunts are measured by velocity-encoded phase-contrast cine MRI employing the breath-hold technique. Thus, MRI provides information relevant to the morphologic diagnosis of congenital heart diseases in most adult patients, and functional measurements obtained by MRI have important prognostic and therapeutic implications for the pre- and postoperative management of CHDs.

References

- Higgins CB, Byrd BF, McNamara M et al. Magnetic resonance imaging of the heart: a review of the experience in 172 subjects. *Radiology* 1985;155:671-679
- Didier D, Higgins CB, Fisher MR, Osaki L, Silverman NH, Cheitlin MD. Congenital heart disease: gated MR imaging in 72 patients. *Radiology* 1986;158:227-235
- Diethelm L, Dery R, Lipton MJ, Higgins CB. Atrial-level shunts: sensitivity and specificity of MR in diagnosis. *Radiology* 1987;162: 181-186
- Gomes A, Lois JF, Williams RG. Pulmonary arteries: MR imaging in patients with congenital obstruction of the right ventricular outflow tract. *Radiology* 1990;174:51-57
- Jacobstein MD, Fletcher BD, Nelson AD, Clampitt M, Alfiidi RJ, Riemenschneider TA. Magnetic resonance imaging: evaluation of palliative systemic-pulmonary artery shunt. *Circulation* 1984;70:650-656
- Fletcher BD, Jacobstein MD. MRI of congenital abnormalities of the great vessels. *AJR* 1986; 146:941-948
- Julsrud PR, Ehman RL, Hagler DJ, Ilstrup DM. Extracardiac vasculature in candidates for Fontan surgery: MR imaging. *Radiology* 1989;173:503-506
- Masui T, Seelos KC, Kersting-Sommerhoff BA, Higgins CB. Abnormalities of the pulmonary veins: evaluation with MR imaging and comparison with cardiac angiography and echocardiography. *Radiology* 1991;181:645-649
- Yoo S-J, Lim TH, Park I-S, et al. MR anatomy of ventricular septal defect in double-outlet right ventricle with situs solitus and atrioventricular concordance. *Radiology* 1991;181:501-505
- Yoo S-J, Seo J-W, Lim TH, et al. Hearts with twisted atrioventricular connections: findings at MR imaging. *Radiology* 1993;

MR Imaging of Congenital Heart Diseases in Adolescents and Adults

- 188:109-113
11. Kersting-Sommerhoff BA, Seelos KC, Hardy C, Kondo C, Higgins SS, Higgins CB. Evaluation of surgical procedures for cyanotic congenital heart disease by using MR imaging. *AJR* 1990;155:259-266
 12. Vick GW III, Rockey R, Huhta JC, Mulvagh SL, Johnston DL. Nuclear magnetic resonance imaging of the pulmonary arteries, subpulmonic region, and aorticopulmonary shunts: a comparative study with echocardiography and angiography. *Am Heart J* 1990;119:1103-1110
 13. Lynch DA, Higgins CB. MR imaging of unilateral pulmonary artery anomalies. *J Comput Assist Tomogr* 1990;14:187-191
 14. Vesely TM, Julsrud PR, Brown JJ, Hagler DJ. MR imaging of partial anomalous pulmonary venous connections. *J Comput Assist Tomogr* 1991;15:752-756
 15. Choe YH, Lee HJ, Kim HS, Ko JK, Kim JE, Han JJ. MRI of total anomalous pulmonary venous connections. *J Comput Assist Tomogr* 1994;18:243-249
 16. Kim TK, Choe YH, Kim HS et al. Anomalous origin of the right pulmonary artery from the ascending aorta: diagnosis by magnetic resonance imaging. *Cardiovasc Intervent Radiol* 1985; 18:118-121
 17. Kersting-Sommerhoff BA, Diethelm L, Teitel DF, et al. Magnetic resonance imaging of congenital heart disease: sensitivity and specificity using receiver operating characteristic curve analysis. *Am Heart J* 1989;118:155-161
 18. Choe YH, Kim YM, Han BK, Park KG, Lee HJ. MR imaging in the morphologic diagnosis of congenital heart disease. *RadioGraphics* 1997;17:403-422
 19. Niezen RA, Helbing WA, Van der Wall EE, Van der Geest RJ, Rebergen SA, De Roos A. Biventricular systolic function and mass studied with MR imaging in children with pulmonary regurgitation after repair for tetralogy of Fallot. *Radiology* 1996;201:135-140
 20. Task force of the European Society of Cardiology, in collaboration with the Association of European Paediatric Cardiologists. The clinical role of magnetic resonance imaging in cardiovascular disease. *Eur Heart J* 1998;19:19-31
 21. Choi YH, Park JH, Choe YH, Yoo SJ. MR imaging of Ebstein's anomaly of the tricuspid valve. *AJR* 1994;163:539-543.
 22. Choe YH, Ko JK, Lee HJ, Kang I-S, Park PW, Lee YT. MR imaging of non-visualized pulmonary arteries at angiography in patients with congenital heart disease. *J Korean Med Sci* 1998; 13:597-602
 23. Ferrari VA, Scott CH, Holland GA, Axel L, Sutton M. Ultrafast three-dimensional contrast-enhanced magnetic resonance angiography and imaging in the diagnosis of partial anomalous pulmonary venous drainage. *J Am Coll Cardiol* 2001;37:1120-1128
 24. Taylor AM, Thorne SA, Rubens MB et al. Coronary artery imaging in grown-up congenital heart disease. Complementary role of magnetic resonance and X-ray coronary angiography. *Circulation* 2000;101:1670-1678.
 25. Wexler L, Higgins CB. The use of magnetic resonance imaging in adults with congenital heart disease. *Am J Card Imaging* 1995;9:15-28
 26. Hartnell GG, Notarianni M. MRI and echocardiography: how do they compare in adults? *Sem Roentgenol* 1998;33:252-261
 27. Hartnell GG, Cohen MC, Meier RA, Finn JP. Magnetic resonance angiography demonstration of congenital heart disease in adults. *Clin Radiol* 1996;51:851-857
 28. Hoppe UC, Dederichs B, Deutsch HJ, Theissen P, Schicha H, Sechtem U. Congenital heart disease in adults and adolescents: comparative value of transthoracic and transesophageal echocardiography and MR imaging. *Radiology* 1996;199:669-677
 29. Pettigrew RI, Oshinski JN, Chatzimavroudis G, Dixon WT. MRI techniques for cardiovascular imaging. *J Magn Reson Imaging* 1999;10:590-601
 30. Reeder SB, Du YP, Lima JAC, Bluemke DA. Advance cardiac MR imaging of ischemic heart disease. *RadioGraphics* 2001;21: 1047-1074
 31. Lee JJ, Tirman PJ, Chang Y et al. The optimization of scan timing for contrast-enhanced magnetic resonance angiography. *Korean J Radiol* 2000;1:142-151
 32. Lee JJ, Chang Y, Kang D-S. Contrast-enhanced magnetic resonance angiography: does the test dose bolus represent the main dose bolus accurately? *Korean J Radiol* 2000;1:91-97
 33. Greene R, Miller SW. Cross-sectional imaging of silent pulmonary venous anomalies. *Radiology* 1986;159:279-281
 34. White CS, Baffa JM, Haney PJ, Campbell AB, NessAvier M. Anomalies of pulmonary veins: usefulness of spin-echo and gradient-echo MR images. *AJR* 1998;170:1365-1368
 35. Hartnell GG, Meier RA. MR angiography of congenital heart disease in adults. *RadioGraphics* 1995;15:781-794
 36. Mirowitz SA, Lee JKT, Gutierrez FR, et al. 'Pseudocoarctation' of the aorta: pitfall on cine MR imaging. *J Comput Assist Tomogr* 1990;14:753-755
 37. Coard KCM, Martin MP. Ruptured saccular pulmonary artery aneurysm associated with persistent ductus arteriosus. *Arch Path Lab Med* 1992;116:159-161
 38. Rominger MB, Bachmann GF, Pabst W, Rau WS. Right ventricular volumes and ejection fraction with fast cine MR imaging in breath-hold technique: applicability, normal values from 52 volunteers, and evaluation of 325 adult cardiac patients. *J Magn Reson Imaging* 1999;10:908-918